First-principles binary diffusion coefficients for H, H_2, and four normal alkanes + N_2

Ahren W. Jasper,[1,*] Eugene Kamarchik,[1] James A. Miller,[2] and Stephen J. Klippenstein[2]
[1]*Combustion Research Facility, Sandia National Laboratories, Livermore, CA 94551*
[2]*Chemical Sciences and Engineering Division, Argonne National Laboratory, Argonne, IL 60439*

(Submitted July 3, 2014)

Collision integrals related to binary (dilute gas) diffusion are calculated classically for six species colliding with N_2. The most detailed calculations make no assumptions regarding the complexity of the potential energy surface, and the resulting classical collision integrals are in excellent agreement with previous semiclassical results for H + N_2 and H_2 + N_2 and with recent experimental results for C_nH_{2n+2} + N_2, n = 2–4. The detailed classical results are used to test the accuracy of three simplifying assumptions typically made when calculating collision integrals: (1) approximating the intermolecular potential as isotropic, (2) neglecting the internal structure of the colliders (i.e., neglecting inelasticity), and (3) employing unphysical R^{-12} repulsive interactions. The effect of anisotropy is found to be negligible for H + N_2 and H_2 + N_2, in agreement with previous quantum mechanical and semiclassical results for small systems. A more significant effect from anisotropy is seen in the collision integrals for larger species at low temperatures. For example, the neglect of anisotropy decreases the diffusion coefficient for butane + N_2 by 15% at 300 K. The neglect of inelasticity, in contrast, is suggested to introduce only very small errors, with a maximum effect of less than 2%. Approximating the repulsive wall as an unphysical R^{-12} interaction is a significant source of error at all temperatures for the weakly interacting systems H + N_2 and H_2 + N_2, with errors as large as 40%. For the normal alkanes in N_2, which feature stronger interactions, the 12/6 Lennard–Jones approximation is found to be accurate, particularly at temperatures above ~700 K where it predicts the full-dimensional result to within 5%. Overall, the typical practical approach of assuming isotropic 12/6 Lennard–Jones interactions is confirmed to be accurate for combustion applications except for weakly interacting systems, such as H + N_2. For these systems, anisotropy and inelasticity can safely be neglected but a more detailed description of the repulsive wall is required for quantitative predictions. A straightforward approach for calculating effective isotropic potentials with realistic repulsive walls is described. An analytic expression for the calculated diffusion coefficient for H + N_2 is presented. This expression includes small adjustments to approximate quantum effects and high-level corrections to the potential energy surface and is estimated to have a 2-sigma error bar of only 0.7%.

*Email: ajasper@sandia.gov

I. INTRODUCTION

Collision integrals, $\Omega^{(l,s)}$, are key components of elementary chemical kinetics calculations and combustion simulations. Physically, they provide the connection between the microscopic intermolecular forces governing individual collisions and the bulk transport properties diffusion, thermal conductivity, and viscosity.[1,2,3] As such, $\Omega^{(l,s)}$ are highly-averaged functions of the intermolecular potential, including averaging over impact parameter, collision energy, relative orientation, etc. Computationally, $\Omega^{(l,s)}$ are most often evaluated in the dilute gas limit (where only binary collisions are important) via Chapman–Enksog theory[4] and assuming an isotropic intermolecular interaction. Implicit in the use of an isotropic intermolecular potential are the additional assumptions that the colliders lack internal structure and that the collisions are elastic (or, equivalently, that the internal degrees of freedom of the colliders are not coupled to the intermolecular degrees of freedom). The isotropic intermolecular potential is often further approximated as a 12/6 Lennard–Jones interaction.

Even with these simplifying assumptions, collision integrals require some care to evaluate with high accuracy, and tables of calculated 12/6 Lennard–Jones collision integrals have been compiled.[5] Use of these tables requires knowledge of the two Lennard–Jones parameters[6] σ and ε, which define the inner turning point at zero asymptotic relative energy and the well depth of the intermolecular potential, respectively. Pure gas Lennard–Jones parameters have been collected[7] for several species (typically extracted from viscosity measurements or estimated), and empirical combining rules may be used to generate binary collision parameters from the pure gas ones.[6] Effective binary isotropic Lennard–Jones parameters may also be calculated directly from the full-dimensional anisotropic intermolecular potential.[8]

Formal solutions of the collision integrals have long been available for classical,[9] semiclassical,[10] and quantum mechanical[11] collisions. Semiclassical and quantal diffusion coefficients (which are inversely related to the collision integral $\Omega^{(1,1)}$) have been calculated using accurate full-dimensional potentials for systems with 2–4 atoms (e.g., Refs. 12,13,14,15,16,17). One notable result from these studies is that the neglect of anisotropy in the intermolecular potential has only a small effect on the computed diffusion coefficients. Monchick et al.[18] provided formal arguments that the effects of

anisotropy and inelasticity on transport properties such as diffusion should be expected to be small in general, but the error associated with the neglect of these details has not been quantified for systems with more than a few atoms.

Significant differences have been observed when comparing semiclassical and quantal diffusion coefficients with those obtained for a classical isotropic 12/6 Lennard–Jones interaction and using tabulated values of σ and ε. These differences cannot be unambiguously attributed to the differences in the dynamical treatments, however, as they may instead arise from differences in the assumed intermolecular potentials (e.g., from differences in the descriptions of the repulsive wall).

Tabulations of (typically classical) collision integrals for other isotropic functional forms exist, including Buckingham or exp/6,[19] Morse,[20] and m/6 Lennard–Jones[5] potentials. These functional forms have more realistic treatments of the repulsive wall than the 12/6 Lennard–Jones functional form but are rarely used. Their infrequent use is most likely due to a lack of knowledge of the additional parameters required to specify these potentials.

Here we calculate classical (1,1) collision integrals and binary diffusion coefficients without making any assumptions about the nature of the intermolecular potential and without neglecting inelasticity. Corrections for non-dilute gases are not considered. Molecular nitrogen is chosen as the bath gas due to its importance as a diluent in combustion experiments and as a proxy for air in combustion systems. The diffusion of six species (H, H_2, CH_4, C_2H_6, C_3H_8, and C_4H_{10}) in N_2 is considered, and trends with respect to system size are identified. The consideration of the normal alkanes in particular is motivated by recent experimental diffusion coefficient measurements of McGivern and Manion.[21]

The error associated with the present use of classical mechanics is likely small, especially at combustion temperatures. For the case of an isotropic 12/6 Lennard–Jones potential, for example, classical collision integrals were shown[11] to be accurate for $T > \varepsilon/k$, which is typically satisfied near room temperature and above. The present classical methods have the significant advantage that they are computationally efficient enough to be applied to large polyatomic systems using high-level full-dimensional potential energy surfaces. The good accuracy of classical mechanics for calculating diffusion coefficients

and of the potential energy surfaces used here is demonstrated via comparisons with previous semiclassical results[13,14] for H + N_2 and H_2 + N_2 as well as comparisons with experimental results[21] for the normal alkanes in N_2.

The principal goal of the present study is to use the validated full-dimensional classical results to quantify the errors associated with the simplifying assumptions identified above, with an emphasis on identifying practical first-principles methods for predicting transport in combustion systems. The term "first-principles" is meant to indicate methods that rely only on calculated or well-known (atomic masses, etc.) parameters and that do not make use of empirically-adjusted or experimental parameters (e.g., tabulated Lennard–Jones parameters). The full-dimensional results are compared with results obtained for calculated isotropic potentials using parameters obtained directly from the full-dimensional potentials with the previously described spherical-averaging method.[8]

We find that detailed treatments of anisotropy, inelasticity, and the repulsive wall are typically not needed for accurate predictions of diffusion coefficients, particularly at combustion temperatures (700–2500 K). Despite its unphysical repulsive wall, the isotropic 12/6 Lennard–Jones potential, along with calculated values of σ and ε, is shown to predict diffusion coefficients for many systems relevant to combustion within ~5%. For polyatomic systems at low temperatures (~300 K), however, the neglect of anisotropy can have non-negligible effects as large as 15%.

A notable exception is the diffusion of H atom, which is often the most important transport property in combustion simulations. The present classical results show that the isotropic 12/6 Lennard–Jones potential cannot be used to accurately treat weakly interacting systems such as H + N_2 and H_2 + N_2 at any temperature and that the principal source of error (as large as 40%) arises from the treatment of the repulsive wall and not from inelasticity or anisotropy. Our previously proposed scheme[8] for calculating σ and ε from full-dimensional intermolecular potentials is generalized here to provide a more detailed description of the repulsive wall within the isotropic approximation. This new method, along with tabulated classical collision integrals for the isotropic exp/6 (Buckingham) potential, provides a convenient first-principles scheme for obtaining accurate collision integrals for weakly interacting systems such as H + N_2.

II. THEORY

For A + B collisions where A and B are molecules with internal structure, the inelastic reduced (1,1) collision integral at some temperature T may be written[2,9]

$$\Omega^{(1,1)*}(T) = \frac{1}{\pi\sigma^2} \sum_{i,j,i',j'} \frac{e^{-\varepsilon_{A,i}}}{Q_A} \frac{e^{-\varepsilon_{B,j}}}{Q_B} \int d\gamma \gamma^3 \mathrm{e}^{-\gamma^2} \int d\phi \sin\chi d\chi (\gamma^2 - \gamma\gamma' \cos\chi) I_{ij}^{i'j'} , \qquad (1)$$

where σ is a reference collision diameter, the indices i and j label the initial (pre-collision) internal states of the reactants A and B with energies $E_{\mathrm{A},i}$ and $E_{\mathrm{B},j}$, respectively, $\varepsilon_{\mathrm{X},i} = E_{\mathrm{X},i}/kT$, k is Boltzmann's constant, Q_A and Q_B are the internal partition functions for the reactants, γ is related to E, the relative A + B collision energy, via $\gamma^2 = \varepsilon = E/kT$, primes denote post-collision properties, ϕ and χ are the azimuth and polar scattering angles, respectively, and $I_{ij}^{i'j'}(\gamma,\phi,\chi)$ is the state-to-state differential scattering cross section. Equation 1 makes no assumptions about the nature of the A + B intermolecular potential.

The binary diffusion coefficient D is related to the (1,1) reduced collision integral via[1,3]

$$D(T) = \frac{3}{16} \frac{(2\pi k^3 T^3/\mu)^{1/2}}{p\pi\sigma^2\Omega^{(1,1)*}} , \qquad (2)$$

where p is the pressure and μ is the reduced mass of the colliders. Equations 1 and 2 assume the dilute gas limit (where only binary collisions are important) and that the colliding partners are governed by thermal distributions.

Equation 1 may be written more transparently for evaluation via Monte Carlo integration. First, we define the thermal populations of the internal states of each of the colliding species $P_{\mathrm{X},i}(T) = \mathrm{e}^{-\varepsilon_{\mathrm{X},i}}/Q_\mathrm{X}$ and the thermal distribution of A + B collision energies $P_\mathrm{rel}(\varepsilon) = \varepsilon\exp(-\varepsilon)$. Then, via a change of integration variables from $d\gamma$ to $d\varepsilon$ and from the solid angle variables $I_{ij}^{i'j'} d\phi \sin\chi d\chi$ to $2\pi b\, db$, where b is the impact parameter, eq 1 becomes

$$\Omega^{(1,1)*}(T) = \frac{1}{\sigma^2} \sum_{i,j,i',j'} P_{\mathrm{A},i} P_{\mathrm{B},j} \int d\varepsilon P_\mathrm{rel} \int db\, b(\varepsilon - \sqrt{\varepsilon\varepsilon'}\cos\chi) . \qquad (3)$$

To evaluate eq 3, ensembles of N trajectories were prepared with initial conditions for A + B collisions sampled from *classical* thermal distributions for $P_{A,i}$, $P_{B,i}$, and P_{rel}, and with the impact parameter sampled uniformly from 0–b_{max}. Full-dimensional classical trajectories were integrated for each member of the ensemble, and the scattering angle χ and final relative energy ε' for each trajectory were calculated. The Monte Carlo expression for $\Omega^{(1,1)*}$ is then

$$\Omega^{(1,1)*}(T) = \frac{b_{max}}{\sigma^2} \sum_{\alpha} b_\alpha (\varepsilon_\alpha - \sqrt{\varepsilon_\alpha \varepsilon'_\alpha}\, \cos\chi_\alpha) / N\,, \tag{4}$$

where the subscript α labels trajectories in the ensemble. Along with the binary collision and thermal assumptions inherent in eq 1, the only additional assumption in eq 4 is that of classical mechanics. Expressions suitable for trajectory-based Monte Carlo evaluations of other collision integrals $\Omega^{(l,s)}$ may be similarly obtained.

Assuming elastic collisions, $\varepsilon'_\alpha = \varepsilon_\alpha$ and eq 4 becomes

$$\Omega^{(1,1)*}(T) = \frac{b_{max}}{\sigma^2} \sum_{\alpha} b_\alpha\, \varepsilon_\alpha (1 - \cos\chi_\alpha) / N\,. \tag{5}$$

The effect of inelasticity on the computed collision integrals was studied by comparing the results of eqs 4 and 5, where eq 5 was evaluated for the same ensembles of full-dimensional trajectories as eq 4. These ensembles do include inelastic collisions, and so the present application of eq 5 only approximates the effect of neglecting inelasticity when evaluating the collision integrals.

The classical trajectory calculations and initial conditions used here are closely related to those for collisional energy transfer, which have been described in detail elsewhere.[22] Briefly, ensemble sizes of N = 1,280,000 for H + N_2 and H_2 + N_2 and N = 128,000 for C_nH_{2n+2} + N_2 were used to evaluate eqs 4 and 5. For these ensemble sizes, the two-sigma bootstrap[23,24] statistical uncertainties were 0.4% for H + N_2 and H_2 + N_2 and 1% for C_nH_{2n+2} + N_2. Initial and final center-of-mass separations (12–17 Å) were chosen such that ε_α and ε'_α were converged to at least seven digits. Equations 4 and 5 converge with respect to the choice of b_{max}, so long as b_{max} is large enough to include non-negligible values of the integrand (we used b_{max} = 10–15 Å). Trajectories were integrated

with a variable step size integrator and an integrator tolerance such that the total energy and total angular momentum were conserved to six digits.

No reference was made to the intermolecular potential when deriving eq 4, and it may be applied generally to full-dimensional intermolecular potentials, i.e., eq 4 is the full-dimensional classical collision integral, including anisotropy and inelasticity. Here we have used our previously parameterized[25] full-dimensional analytic potentials for $C_xH_y + N_2$ and two newly fitted analytic potentials for $H + N_2$ and $H_2 + N_2$.

The "universal" $C_xH_y + N_2$ potential employs the separable pairwise approach for the intermolecular potential with atom-atom interactions obtained from a previous parameterization of the $CH_4 + N_2$ system.[26] The use of CH_4 + M pairwise intermolecular parameters as universal parameters for larger hydrocarbons was tested[25] in energy transfer calculations for C_2H_y + He and was shown to be accurate within the statistical uncertainty of those calculations (~10%). In another study, the universal C_xH_y + M potentials were used to calculate 12/6 Lennard–Jones collision rates for a variety of baths within ~10% of those based on tabulated values for several systems as large as octane.[8,25]

The $H + N_2$ potential energy surface was obtained by fitting a grid of 1425 counterpoise corrected QCISD(T)/CBS interaction energies, where the CBS limit was calculated from the aug-cc-pVTZ and aug-cc-pVQZ basis sets. The separable pairwise[26] functional form was used, with H–N interactions modeled using the cutoff exp/6 (Buckingham) formula. A previously obtained[26] potential energy curve for isolated N_2 was used for the N–N interaction.

The $H + N_2$ intermolecular potential has only 4 adjustable parameters, the mean unsigned fitting error to the 1425 QCISD(T)/CBS interaction energies was 14 cm^{-1} for energies below 3000 cm^{-1}. The mean unsigned fitting error cannot readily be interpreted as a measure of the quality of the fit, however, as the functional form fits the long-range data with small (< 1 cm^{-1}) errors by construction, while errors can be as large ~1000 cm^{-1} for strongly repulsive interactions. The mean unsigned fitting error therefore depends arbitrarily on the relative amounts of long-range and short-range data included in the fit. Furthermore, the mean unsigned error is not a good indicator of the accuracy of using this fitted potential in the present dynamical application. As discussed previously in the context of energy transfer calculations,[26] it is more useful to characterize the fitted

potential in terms of its ability to reproduce small interaction energies (i.e., those associated with the van der Waals well) as well as its ability to reproduce the *range* of the repulsive wall at shorter center-of-mass separations. The accuracy of the newly fitted H + N_2 potential for the present application is further discussed from this perspective in Sec. III.

For H_2 + N_2, the fitted potential was obtained using permutationally invariant polynomials[27,28,29] in Morse variables, $y_{ij} = \exp(-a\, r_{ij})$, where r_{ij} is the distance between atoms i and j. We again made the separable approximation and fit only the intermolecular potential using permutationally invariant polynomials. This approach has the advantage that different levels of theory could be used to describe the isolated potentials for H_2 and N_2 and the intermolecular potential. The one-dimensional diatomic potential curves were taken from previously-described[26] analytic fits to high-level ab intio energies for those systems. The intermolecular potential was fit to 25,000 counterpoise corrected MP2/CBS interaction energies, where the CBS limit was calculated from the aug-cc-pVDZ and aug-cc-pVTZ basis sets. This level of theory was found to agree well with the more computationally-demanding counterpoise corrected QCISD(T)/CBS method and with two-point CBS extrapolations based on the aug-cc-pVTZ and aug-cc-pVQZ basis sets.

As discussed in detail in the supporting information of Ref. 28, the permutationally invariant polynomial representation of the intermolecular potential is not guaranteed to go to zero as H_2 and N_2 separate due to "unconnected" terms such as $y_{ij}\, y_{kl}$, where i and j label atoms in one molecule and k and l label atoms in the other. To enforce the desired asymptotic behavior, the interaction energy was fit using 4^{th}-order permutationally invariant polynomials from which terms that did not include only H–N distances were removed.[28] With these terms removed, 22 linear parameters remained in the functional form for the intermolecular potential. The root-mean-square error of the fit was 18 cm^{-1} for all of the data included in the fit and only 5 cm^{-1} for data below 2000 cm^{-1}. The quality of the fitted H_2 + N_2 potential for the present dynamical application is further discussed in Sec. III.

The results of the full-dimensional trajectory calculations (eq 4) are compared with results obtained using isotropic potentials, including the m/6 Lennard–Jones potential[5]

$$V(R) = \frac{\varepsilon}{(6/m)^{6/(m-6)} - (6/m)^{m/(m-6)}}\left[\left(\frac{\sigma}{R}\right)^{m} - \left(\frac{\sigma}{R}\right)^{6}\right], \tag{6}$$

and the exp/6 potential[19]

$$V(R) = \frac{\varepsilon}{1 - 6/\alpha}\left[\frac{6}{\alpha}e^{\alpha(1-R/R')} - \left(\frac{R'}{R}\right)^{6}\right], \tag{7}$$

where R' is the value of R for which V is a minimum; σ is related to R' by setting $V = 0$ and $R = \sigma$ in eq 7. The classical reduced collision integrals for these potentials were interpolated from those reported in previously compiled tables.[5,19]

The use of isotropic potentials beyond the 12/6 Lennard–Jones functional form requires additional information about the repulsive wall to determine the value of the third parameter (m in eq 6 or α in eq 7). Here, we generalize our previously described[8] "orientation-averaging with one-dimensional optimizations" scheme to obtain more information about the repulsive wall. In the method, the two colliding species are oriented randomly with respect to one another, and one-dimensional optimizations are performed with respect to their center-of-mass distance. Previously,[8] two optimizations were carried out: the minimum energy $-V'$ was located, and the center of mass distance for the inner turning point $R(V = 0)$ was located, where the zero of energy in V is defined as the asymptotic A + B energy. This process was repeated for many uniformly sampled A + B orientations, and the calculated Lennard–Jones parameters were obtained $\sigma \equiv \langle R(V = 0)\rangle$ and $\varepsilon \equiv \langle V'\rangle$, where the brackets denote averages over the sampled orientations. This method was shown to predict Lennard–Jones collision rates (typically) within 10% of those based on tabulated Lennard–Jones parameters for a wide variety of systems.[8] Here, we generalize this procedure to also obtain $\bar{R}(V) \equiv \langle R(V)\rangle$ for $V > 0$, where $\bar{R}(0) = \sigma$ as defined above. This approach is equivalent to determining the hypervolume of the full-dimensional intermolecular potential defined by the equipotential surface V and then computing the diameter $\bar{R}(V)$ for a hypersphere (or isotropic interaction) of the same volume. The calculated values of $\bar{R}(V)$ for $V > 0$ are used to determine m and α, as discussed below.

III. RESULTS AND DISCUSSION

A. $H + N_2$

Lennard–Jones parameters for $H + N_2$ were calculated using the spherical-averaging method of Ref. 8. The fitted potential predicts $\varepsilon = 26.1$ cm^{-1} and $\sigma = 3.36$ Å in excellent agreement with direct QCISD(T)/CBS results ($\varepsilon = 27.0$ cm^{-1} and $\sigma = 3.35$ Å). One tabulation of Lennard-Jones parameters used extensively in combustion modeling[7] lists these parameters as $\varepsilon = 82.7$ cm^{-1} and $\sigma = 2.84$ Å, where the usual geometric and arithmetic mean combining rules[6] have been used to obtain the $H + N_2$ parameters from the pure gas ones for H and N_2. These tabulated parameters do not bear any obvious relationship with the calculated intermolecular potential, with differences well outside the expected accuracy of the counterpoise corrected QCISD(T)/CBS method.

The repulsive wall for $H + N_2$ was characterized using the fitted surface and the spherical-averaging method discussed above to calculate $\bar{R}(V)$ for $V > 0$. These results are shown in Fig. 1(a), along with direct QCISD(T)/CBS calculations of $\bar{R}(V)$ at four energies. Again, the fitted surface accurately reproduces the QCISD(T)/CBS results. Also shown in Fig. 1(a) are the 9/6 and 12/6 Lennard-Jones potentials for the calculated values of $\varepsilon = 26.1$ cm^{-1} and $\sigma = 3.36$ Å. The calculated repulsive wall is softer and shorter-ranged than either of the Lennard–Jones potentials. The 9/6 repulsive wall, while more accurate than the 12/6 repulsive wall, is still significantly longer-ranged and harder than the calculated potential. The repulsive Lennard–Jones exponent could be further optimized to $m = 7$, but the resulting fit remains qualitatively harder than the calculated potential.

As expected, the intermolecular potential is more accurately represented using an exp/6 (Buckingham) isotropic potential. The exp/6 potential shown in Fig. 1(a) was obtained for $H + N_2$ by fixing the well depth and $V = 0$ turning point (i.e., ε and σ) at their calculated values for the fitted potential and optimizing the single remaining parameter ($\alpha = 11.6$) to fit the calculated repulsive wall. Unlike the Lennard–Jones potentials, the fitted exp/6 potential accurately reproduces both the range and softness of the repulsive wall up to at least 2500 cm^{-1}.

The 12/6 Lennard–Jones potential based on the tabulated[7] parameters for H + N_2 (ε = 82.7 cm^{-1} and σ = 2.87 Å) is also shown in Fig. 1(a). Despite the significant differences in the well depth and the V = 0 turning point, we note that the range of the repulsive interaction agrees with the calculated intermolecular potential around ~1000 cm^{-1}.

Reduced (1,1) collision integrals were calculated by interpolating from tabulations of collision integrals for the isotropic Lennard–Jones and exp/6 potentials shown in Fig. 1(a). These are compared in Fig. 1(b) with the results of the full-dimensional trajectories (eq 4). Also shown are the full-dimensional semiclassical scattering results of Stallcop et al.,[13] who used a high-quality potential energy surface based on counterpoise corrected multireference configuration interaction energies.

Although we are principally concerned with quantifying the accuracy of the calculated values of D, it is more convenient to present and discuss $\Omega^{(1,1)*}$. Differences in the methods' predictions are more readily seen when plotting $\Omega^{(1,1)*}$, which varies by only a factor of ~2 from 300–3000 K, while D varies by two orders of magnitude over the same temperature range. We note that care must be taken when comparing reduced collision integrals obtained from different sources (theory, experiment, tabulation, etc…), as they will generally have been reduced to different reference hard-sphere values, i.e., to different values of σ. Reduced collision integrals may be trivially rescaled (or reduced) to any other reference $\bar{\sigma}$ via $\bar{\Omega}^{(1,1)*} = \frac{\sigma^2}{\bar{\sigma}^2}\Omega^{(1,1)*}$. The product $\sigma^2\Omega^{(1,1)*}$ is invariant to the choice of σ, and it is this product that appears when calculating physical properties, such as D in eq 2. To enable direct comparisons of the present collision integrals obtained from different sources, all of the results shown in Fig. 1(b) have been reduced to the calculated value of $\bar{\sigma}$ = 3.36 Å. By using a consistent value of $\bar{\sigma}$ for all the methods, the *relative* differences in the curves in Fig. 1(b) are the same as those that would be observed for D, although the order is reversed due to the inverse relationship between D and $\sigma^2\Omega^{(1,1)*}$. Again, a method's relative error in $\bar{\Omega}^{(1,1)*}$ may be interpreted as its relative error in D. This is only true when collision integrals for the different methods have been scaled to a consistent choice for $\bar{\sigma}$.

As shown in Fig. 1(b), the full-dimensional classical trajectory results are in excellent agreement with the semiclassical scattering results of Stallcop et al.,[13] differing by less than 2% below 1500 K and by up to only 6% at 3000 K. These small differences are most likely due to small differences in the potential energy surfaces used in the two calculations. It is less likely that these differences are due to the different dynamical treatments employed. The use of classical mechanics may be motivated for this system by noting that quantum effects are expected to be small when $T^* = kT/\varepsilon > 1$,[11] and for this system $T^* = 8 - 77$ for $T = 300 - 3000$ K.

The reduced collision integral for the calculated 12/6 Lennard–Jones potential does not agree well with the full-dimensional classical result and is too high by 10–40% from 300–3000 K, as shown in Fig. 1(b). The use of the 9/6 Lennard–Jones potential improves the agreement somewhat, but differences of up to 20% remain at high temperature. These results correlate qualitatively with the accuracy of the two methods' description of the repulsive wall shown in Fig. 1(a).

The reduced collision integral for the calculated isotropic exp/6 potential—which accurately fits the calculated spherically-averaged repulsive wall as noted above and as shown in Fig. 1(a)—agrees quantitatively with the full-dimensional result, differing within the 0.4% 2-sigma statistical uncertainties for all but the high-temperature results where the differences are less than 3%. Stallcop et al.[13] found that semiclassical collision integrals for H + N_2 calculated using an isotropically-averaged potential agreed well with their full-dimensional semiclassical results, and the present classical calculations also show this result.

The neglect of the internal structure of N_2 for this system may be further motivated by noting that the effect of inelasticity in H + N_2 collisions is negligible. The predicted reduced collision integral obtained using eq 4 differs from the one obtained using eq 5 by < 0.5% for the entire temperature range considered here.

Next, we compare the reduced collision integral for the *tabulated* 12/6 Lennard–Jones potential with the calculated full-dimensional result (eq 4). While the empirically-adjusted 12/6 Lennard–Jones parameters result in a qualitatively inaccurate intermolecular potential (cf. Fig. 1(a)), the resulting reduced collision integral nonetheless reproduces the full-dimensional result within 10% for temperatures up to

2000 K and with an error of just 20% at 3000 K. This is a significant improvement relative to the reduced collision integral for the *calculated* 12/6 Lennard–Jones potential. Clearly, the empirically-determined tabulated Lennard–Jones parameters cannot be physically motivated based on the H + N_2 intermolecular potential. Instead, the empirical parameters should be interpreted as (fairly accurate) effective collision integral parameters within the restriction of the unphysical 12/6 Lennard–Jones functional form.

Notably, no choice of σ and ε can be made that quantitatively reproduces the calculated full-dimensional reduced collision integral over the entire temperature range considered within the restriction of the 12/6 Lennard–Jones functional form. In contrast, the exp/6 functional form—which has only one additional parameter that may be readily calculated using the modified spherical-averaging scheme presented above—quantitatively predicts the calculated full-dimensional reduced collision integral over the entire temperature range considered.

Finally, due to its importance in combustion modeling, an improved theoretical value of $D(T)$ for H + N_2 was obtained and a theoretical error analysis was performed, as detailed in the Appendix. Briefly, the results of eq 4 were corrected for small systematic errors associated with quantum effects and with errors in the potential energy surface. An analytic three-parameter expression for D evaluated at 1 atm was obtained,

$$D_{1\mathrm{atm}}(T) = 1.111\ (T/300\ \mathrm{K})^{1.801}\ \exp(36.49\ \mathrm{K}/T)\ \mathrm{cm}^2/\mathrm{s}, \qquad (8)$$

that reproduces the improved calculated values of D to better than 0.4% from 300–3000 K. This expression was assigned 2-sigma theoretical error bars of 0.7%. The improved calculated values of D are lower than the results of Stallcop et al.[13] by 3% at 300 K and are higher by 5% at 3000 K. It may be more convenient to express eq 8 as a set of effective exp/6 parameters. Diffusion coefficients calculated for the empirical exp/6 parameters ε = 28.50 cm^{-1}, σ = 3.312 Å, and α = 11.45 reproduce eq 8 to better than 0.7% from 300–3000 K.

B. H_2 + N_2

Overall, trends in the results for H_2 + N_2 are similar to those discussed above for H + N_2, and we focus here on notable differences. Most importantly, the treatment of the repulsive wall has a less significant effect on the computed reduced collision integral for

$H_2 + N_2$ than for $H + N_2$. As shown in Fig. 2(a), the calculated repulsive wall for $H_2 + N_2$ is fairly well-described by the 9/6 Lennard–Jones potential, with an optimized repulsive Lennard–Jones exponent of $m = 8.5$. The optimized exp/6 parameter for $N_2 + H_2$ is $\alpha = 12.5$, which somewhat more accurately describes the repulsive wall at high energies than the 9/6 and 8.5/6 potentials. For this system, the calculated Lennard–Jones parameters ($\varepsilon = 45.0$ cm^{-1} and $\sigma = 3.32$ Å) agree very well with tabulated[7] ones ($\varepsilon = 42.3$ cm^{-1} and $\sigma = 3.30$ Å), and in both cases the 12/6 Lennard–Jones repulsive wall is harder and longer-ranged than the calculated repulsive wall.

As shown in Fig. 2(b), the full-dimensional trajectory results are in excellent agreement with the semiclassical scattering results of Stallcop et al.[14] with differences of less then 3%. Again, these differences are most likely due to small differences in the potential surfaces. The excellent agreement between the present classical and previous semiclassical results may be motivated by the criterion $T^* > 1$ describing the threshold below which quantum effects may be seen in the collision integrals,[11] where here $T^* = 5 – 46$.

The reduced collision integral for the calculated exp/6 isotropic potential is in near quantitative agreement with the full dimensional results (agreeing to better than 2%), which again supports the conclusion that anisotropy and inelasticity may be safely neglected for small (3–4 atom) systems.

The reduced collision integral for the calculated 12/6 Lennard–Jones potential is in relatively poor agreement with the higher-level results, with errors up to 16% at high temperatures. These errors are smaller than those for $H + N_2$, but we may nonetheless again conclude that the unphysical 12/6 Lennard–Jones repulsive wall is not suitable for quantitative predictions for this system. The relative errors in the computed reduced collision integrals are again clearly related to the accuracy of the descriptions of the repulsive walls shown in Fig. 2(a). The reduced collision integral for the three-parameter exp/6 isotropic potential along with calculated values of σ, ε, and α quantitatively predicts the full-dimensional result for this weakly interacting system.

The reduced collision integral for the tabulated 12/6 Lennard–Jones potential are in somewhat better agreement with the full-dimensional results than those for the

calculated 12/6 Lennard–Jones potential, particularly at low temperatures, but errors as large as 13% remain at high temperature.

C. $C_nH_{2n+2} + N_2$

Next we consider the binary diffusion of C_nH_{2n+2} in N_2 for n = 1–4, which has been recently studied both experimentally and computationally. McGivern and Manion[21] measured binary diffusion coefficients for ethane, propane, and butane in N_2 at temperatures up to 723 K. Chae et al.[30] used large-scale molecular dynamics simulations consisting of 3300 molecules to evaluate diffusion coefficients from 500–1000 K for normal alkanes as large as $C_{16}H_{34}$ in N_2. The diffusion coefficients were obtained from the molecular dynamics simulations using the Green–Kubo formalism,[31] which can in principle be used to model non-binary collisions. These effects are likely negligible at the conditions considered in their study and in the experiments of McGivern and Manion[21] and are explicitly neglected in the present calculations. The present approach (eq 4) is therefore closely related to one used in Ref. 30, as both calculations rely on simulating large numbers of full-dimensional classical binary collisions.

Relative to the large-scale Green–Kubo molecular dynamics simulations, eq 4 is more readily applied using high-level potential energy surfaces. The present method requires the computation of ensembles of independent short-time (~2 ps) classical trajectories for just *two* colliding molecules. In contrast, the Green–Kubo calculations involve the simultaneous simulation of thousands of molecules for much longer timescales (14 ns in Ref. 30). The potential energy surface used by Chae et al.[30] features empirical pairwise intermolecular atom–atom 12/6 Lennard–Jones interactions, which were fitted to reproduce various experimental properties that are sensitive to the intermolecular forces. The $C_nH_{2n+2} + N_2$ potential energy surface used here has not been empirically adjusted to fit any bulk properties and is instead based on calculated ab initio intermolecular energies.[26]

Lennard–Jones parameters σ and ε for methane, ethane, propane, and butane + N_2 were previously calculated[8] using the spherical-averaging method and were shown to be in fairly good agreement with the tabulated experimental Lennard–Jones parameters of Tee et al.,[32] where, again, the usual combining rules were used. Here, these calculations

were extended to include $\bar{R}(V)$ for $V > 0$, and the calculated spherically-averaged repulsive walls are shown in Figs. 3(a)–6(a). These are compared with 9/6 and 12/6 Lennard–Jones potentials obtained for the calculated values of σ and ε. Unlike H + N_2 and H_2 + N_2, the calculated 12/6 Lennard–Jones potential fairly accurately reproduces the calculated spherically-averaged repulsive interactions for all four of the normal alkanes in N_2. The 9/6 Lennard–Jones potential, in contrast, is too short-ranged and too soft, with larger differences for the larger alkanes. Isotropic exp/6 potentials for each system were obtained using the calculated values of σ and ε and optimizing α = 14.2, 15.3, 16.2, and 16.5 to reproduce $\bar{R}(V)$ for methane, ethane, propane, and butane + N_2, respectively. For all four systems, the exp/6 potentials accurately reproduce the calculated repulsive wall energies up to at least 2500 cm^{-1}.

Reduced collision integrals for methane, ethane, propane, and butane + N_2 are shown in Figs. 3(b)–6(b). The full-dimensional calculated reduced collision integrals are in quantitative agreement with the experimental results of McGivern and Manion[21] for all three systems and for the entire temperature range studied experimentally. The differences are smaller than the present 2-sigma statistical uncertainties (1%) for ethane + N_2 and butane + N_2 and are just ~2% for propane + N_2. This excellent agreement again supports the present use of classical mechanics, as there is no apparent evidence of missing quantum effects in these comparisons at low temperature despite the room temperature values of T^* approaching 1 for these systems. We emphasize that no empirical adjustments have been made to the potential energy surfaces used here, and that the present calculations come entirely from first principles.

The previous calculated results of Chae et al.[30] are also in quantitative agreement with the experimental results for butane + N_2 with larger (but still relatively small) differences for the smaller alkanes. The results of eq 4 and those of Chae et al.[30] differ by up to 9% for methane + N_2. These differences most likely arise from differences in the potential energy surfaces used in the two studies, although differences may arise from the dynamical treatments as well.

Next, we quantify the effects of inelasticity, anisotropy, and the treatment of the repulsive wall on the computed reduced collision integrals for these polyatomic systems. These effects have not been well studied for systems larger than a few atoms. Even for

the largest system considered here, butane + N_2, the effect of inelasticity is small, with the results of eqs 4 and 5 differing from one another by no more than 2% (and typically by less than 0.5%). Comparing the full-dimensional results with those obtained for the calculated isotropic exp/6 potential, we may therefore interpret any differences as arising entirely from the treatment of anisotropy in the intermolecular potential.

We note that our calculated exp/6 potential, although reasonable and well-defined, is not unique and that other reasonable isotropic potentials may be defined. Because any discussion of the effect of anisotropy requires a reference isotropic potential, the quantification of this effect is therefore necessarily somewhat arbitrary. Our present choice of using the calculated exp/6 reference potential is supported by the excellent agreement demonstrated above between its reduced collision integrals and those of the present full-dimensional classical and previous full-dimensional semiclassical results of Stallcop et al. for H + N_2 and H_2 + N_2, systems where the effect of anisotropy was previously reported to be small. Importantly, the present approach of comparing the full-dimensional results of eq 4 with those of the calculated exp/6 and 12/6 potentials allows us to separately quantify the effects of anisotropy and those related to the treatment of the repulsive wall.

Unlike for the 3- and 4-atom systems considered above, the effect of anisotropy for C_nH_{2n+2} + N_2 is not negligible, with the largest effect at low temperatures. At room temperature for example, the neglect of anisotropy increases the reduced collision integral by 7–15% for n = 1–4. Notably, a detailed treatment of anisotropy is required to obtain quantitative agreement with the available results from 300–700 K discussed above. The effect of anisotropy is smaller at higher temperatures, varying from 3–7% at 1000 K to just 2% at 1500 K and above.

Next, we consider the treatment of the repulsive wall. The reduced collision integrals for the calculated 12/6 Lennnard–Jones potential are in close agreement with those based on the exp/6 potential, as suggested by the potential curves in Figs. 3(a)–6(a). Results for the calculated 9/6 Lennnard–Jones potential are lower and in better agreement with the full-dimensional theoretical and experimental results. The present comparisons show that the improved accuracy of the 9/6 potential depends on a fortuitous cancellation of the errors arising from both the neglect of anisotropy and the inaccurate description of

the repulsive wall. While this is perhaps a useful practical result for improving the treatment of transport properties in existing kinetics codes, it is not clear if this cancellation can be relied upon in general.

We emphasize that, while not quantitative, the 12/6 Lennard–Jones collision integrals for C_nH_{2n+2} + N_2 obtained using calculated values of σ and ε are in reasonably good agreement with available experimental results and with the present full-dimensional classical results, particularly at high temperatures. This result may be used to justify the usual approach of using 12/6 collision integrals in detailed combustion applications. An accuracy of ~5% in the transport properties is likely suitable for many combustion applications, and this threshold is achieved for the calculated isotropic 12/6 Lennard–Jones potential above ~700 K for the C_nH_{2n+2} + N_2 systems—i.e., detailed treatments of anisotropy and of the repulsive wall are not required. Tabulations of σ and ε, such as our previous tabulation of calculated Lennard–Jones parameters,[8] may therefore be reliably used along with isotropic 12/6 Lennard–Jones collision integrals for most systems at conditions relevant to combustion. Of course, as discussed above, important exceptions are weakly interacting systems, such as the H + N_2 system, which is more accurately described using exp/6 collision integrals.

Interestingly, the full-dimensional classical results of eq 4 and those of Chae et al.[30] show different trends with respect to the effect of anisotropy and system size for the normal alkanes in N_2. As shown in Fig. 5 from Ref. 30, the full-dimensional classical calculations of Chae at al. indicate that the neglect of anisotropy *decreases* the collision integral (and therefore increases the diffusion coefficient). They show that such an effect can be quite significant for large species, such as $C_{16}H_{34}$. This can be seen in the present comparisons of their results as well, where the Chae et al. reduced collision integrals are larger (and sometimes less accurate) than the reduced collision integrals for the tabulated 12/6 Lennard–Jones potentials for all four systems. Comparing their molecular dynamics results with the present results for the calculated exp/6 or 12/6 isotropic potentials, however, would instead lead to the interpretation that the neglect of anisotropy decreases the collision integral for methane, has a small effect for ethane, but increases the collision integral for propane and butane. Neither of these trends agrees with the trend identified in the present calculations, where we find that the neglect of anisotropy consistently

increases the calculated collision integrals, with more significant effects at lower temperatures and for larger systems.

Finally, we consider the accuracy of using 12/6 Lennard–Jones collision integrals along with tabulated (empirical) parameters σ and ε. As observed above for H + N_2 and H_2 + N_2, the reduced collision integrals for the empirical 12/6 Lennard–Jones potentials for C_nH_{2n+2} + N_2 are systematically lower and more accurate than those for the calculated 12/6 Lennard–Jones potentials. Neither of the 12/6 Lennard–Jones collision integrals accurately reproduces the shape of the experimental or full-dimensional calculated collision integrals over the entire temperature range considered. As discussed above, this deficiency arises from the neglect of anisotropy and is therefore unavoidable within the constraint of using isotropic collision integrals. The detailed temperature-dependence of the full-dimensional calculated collision integrals cannot be quantitatively reproduced using the 12/6 Lennard–Jones potential for any choice of parameters σ and ε. Because of this limitation, empirically-optimized parameters σ and ε will differ from calculated ones in such a way as to compensate for the neglect of anisotropy in the collision integrals. Again, existing tabulations of empirical parameters σ and ε should be interpreted as effective parameters within the constraint of the isotropic 12/6 Lennard–Jones potential; these parameters will not necessarily have any clear relationship with the calculated intermolecular potential. Furthermore, empirically-optimized values of σ and ε will generally depend on the temperature range over which they were optimized, such that experimental determinations of 12/6 Lennard–Jones parameters at room temperature may not be suitable for combustion applications.

IV. SUMMARY AND CONCLUSIONS

Full-dimensional classical collision integrals $\Omega^{(1,1)}$ relevant to the binary diffusion coefficient D were calculated for six systems colliding with N_2 using Monte Carlo sampling and ensembles of classical trajectories (eq 4). These calculations made no simplifying assumptions about the potential energy surface, and here we used analytic full-dimensional potential energy surfaces fitted to reproduce ab initio interaction energies. The present method for calculating $\Omega^{(1,1)}$ (or equivalently D) therefore comes from first-principles, requiring no empirical or experimental information.

To more clearly show differences in the various calculated and measured values, $\Omega^{(1,1)}$ was presented in detail in Sec. III instead of D. The *relative* errors and differences in $\Omega^{(1,1)}$ are the same as those in D, and in this summary we focus on the accuracy of the calculated values of D. The first-principles calculated values of D were in excellent agreement with available experimental[21] values for ethane, propane, and butane in N_2, with relative differences of less than 2%. These differences are similar to the combined reported experimental and present statistical uncertainties. Excellent agreement was also found between the present calculated values of D and the previous semiclassical values of Stallcop et al.[13,14] for H + N_2 and H_2 + N_2. Although both adjustments were small, the present calculation of D for H + N_2 was improved by approximately adjusting for quantum effects and for high-level quantum chemistry corrections to the potential energy surface. An analytic expression for D based on the improved calculated results for H + N_2 was reported (eq 8) that differs by a few percent from that of Stallcop et al.[13]

Together, these results support the 50-year old suggestion[11] that classical collision integrals may be expected to be very accurate for molecular systems at room temperature and above. Specifically, the criterion for accurate classical collision integrals suggested in Ref. 11 was $T^* > 1$. We note that the largest value of ε considered here was 137 cm^{-1} for butane + N_2, for which $T^* = 1.5$ at 300 K, close to the $T^* = 1$ threshold identified in Ref. 11. Larger species, species with permanent dipoles, etc., will feature stronger interactions, larger values of ε, and smaller values of T^*. Detailed quantal/classical comparisons may reveal room temperature quantum effects for these more strongly interacting systems, although these effects may be mitigated by the mass-dependence of the quantum correction, as discussed in Ref. 11.

The full-dimensional classical results were used to quantify the accuracy of simplifying assumptions often made when calculating collision integrals and diffusion coefficients, with the goal of identifying practical first-principles approaches for generating accurate transport parameters for combustion applications. Comparing the results of eqs 4 and 5, the effect of collisional inelasticity on the computed values of D was studied. As anticipated generally,[18] the effect of explicitly including inelasticity was suggested to be negligible for all of the systems considered here.

To quantify the effect of neglecting anisotropy when calculating D, the full-dimensional results of eq 4 were compared with those for calculated isotropic exp/6 (Buckingham) potentials. The three exp/6 parameters were determined for each system by calculating the Lennard–Jones parameters σ and ε from the full-dimensional potential as described previously[8] and the exponential range parameter α by spherically averaging over the full-dimensional repulsive wall. The calculated exp/6 potentials were shown to reproduce the range and softness of the spherically-averaged repulsive walls for all the systems considered here more accurately than the 9/6, 12/6, or optimized m/6 Lennard–Jones potentials.

The neglect of anisotropy in the intermolecular potential was shown to introduce non-negligible errors in the calculated diffusion coefficients for polyatomic systems at low temperatures. At room temperature, for example, the neglect of anisotropy decreased the predicted diffusion coefficient by 15% for butane + N_2. Notably, detailed treatments of anisotropy were needed to achieve quantitative agreement with McGivern and Manion's[21] measured diffusion coefficients at 300–700 K. At higher temperatures, the error associated with the neglect of anisotropy was found to be small. The previously reported result[12,13,14,15,16,17] that anisotropy could be safely neglected at all temperatures for 3- and 4-atom systems was confirmed here in the classical results for H + N_2 and H_2 + N_2. This result, however, evidently does not hold for polyatomic systems at low temperatures. This conclusion agrees with that of Ma et al.,[33] who recently quantified the effect of anisotropy in quantal collisional energy transfer calculations for CH_3 + He.

By comparing collision integrals for the calculated isotropic 12/6 Lennard–Jones and exp/6 potentials, the error associated with the treatment of the repulsive wall was quantified. An accurate description of the repulsive wall was necessary to quantitatively predict D for the weakly interacting systems H + N_2 and H_2 + N_2. Specifically, the use of the 12/6 Lennard–Jones potential resulted in under-predicted diffusion coefficients by 15–40% from 300–3000 K for H + N_2. The use of a calculated exp/6 potential is nearly as simple as the more frequently employed 12/6 Lennard–Jones potential and is significantly more accurate for weakly interacting systems.

Diffusion coefficients based on empirically determined 12/6 Lennard–Jones parameters were considered. The empirical values of σ and ε generally bear no

straightforward relationship with the intermolecular potential and with the calculated values of σ and ε. The empirical parameters should instead be interpreted as effective parameters that compensate for errors arising from the neglect of anisotropy and/or from the inaccurate treatment of the repulsive wall within the restriction of the 12/6 Lennard–Jones functional form.

Despite the errors enumerated above, we emphasize that even the simplest first-principles calculations considered here are likely sufficiently accurate for determining the majority of the large number of transport parameters required for detailed chemical kinetic combustion simulations. Specifically, diffusion coefficients obtained using calculated 12/6 Lennard–Jones potentials were shown to agree with those obtained from eq 4 within ~5% for the normal alkanes in N_2 at temperatures above ~700 K. This is likely representative of the general accuracy of this approach for most systems and conditions relevant to combustion. (Errors were larger at 300 K, suggesting that more detailed theoretical methods for calculating transport properties may be required when building models for lower-temperature applications such as atmospheric chemistry.) A very important exception for combustion applications is the diffusion of H in N_2, which, as noted above, is not well described by the 12/6 Lennard–Jones potential and requires the use of a potential with a more realistic repulsive wall such as the exp/6 potential. This is likely a general result for weakly interacting systems, and we showed that the three exp/6 parameters may be straightforwardly calculated from the full-dimensional potential via a spherical-averaging approach. An analytic expression for the calculated value of D for H + N_2 was presented and assigned 2-sigma error bars of only 0.7%.

In summary, for building practical databases of transport properties for combustion (T > 700 K) the classical isotropic 12/6 Lennard–Jones model may be reliably used for most systems, while the classical isotropic exp/6 model should be used for weakly interacting systems. Tabulated collision integrals are available for both models, and the required two (σ and ε) or three parameters (σ, ε, and α) may be calculated directly from the full-dimensional interaction potential. When more accurate results are required, trajectory-based Monte Carlo sampling along with ab initio potential energy surfaces may be used to calculate classical transport properties with very high accuracy.

Acknowledgements

This work is supported by the Division of Chemical Sciences, Geosciences, and Biosciences, Office of Basic Energy Sciences, U.S. Department of Energy. Sandia is a multiprogram laboratory operated by Sandia Corporation, a Lockheed Martin Company, for the United States Department of Energy under Contract No. DE-AC04-94-AL85000. The work at Argonne was supported under Contract No. DE-AC02-06CH11357 as part of the Argonne-Sandia Consortium on High-Pressure Combustion Chemistry (FWP # 59044). Software development was supported by the AITSTME project as part of the Predictive Theory and Modeling component of the Materials Genome Initiative.

Appendix. Theoretical error analysis and an improved calculated value of *D* for H + N_2

Here we present a detailed theoretical error analysis for the calculated value of *D* for H + N_2. This analysis is used both to improve the calculated value of *D* and to provide first-principles error bars. One may identify three sources of error in the calculations for H + N_2 described in Sec. III.A: (1) the use of classical mechanics, (2) Monte Carlo statistical uncertainties in eq 4 or, equivalently, numerical uncertainties associated with the quadratures used to evaluate the previously tabulated collision integrals for the isotropic potentials, and (3) errors in the potential energy surface.

We estimated the quantum correction to *D* for H + N_2 based on the detailed comparison of quantal and classical results for the 12/6 Lennard–Jones potential given in Ref. 11. Using Fig. 5 of Ref. 11 and the present calculated values of σ and ε, the quantum correction was estimated to increase *D* by 0.8% at 300 K, 0.3% at 700 K, and < 0.1% above 1250 K. These relative corrections based on the 12/6 Lennard–Jones potential were assumed to also apply to the results of eq 4.

As mentioned above, 2-sigma statistical error bars for eq 4 were estimated via the bootstrap method and are 0.4%. This error is likely larger than other numerical errors associated with the trajectory calculations. Quadrature errors for the tabulated exp/6 collision integrals from Ref. 19 were reported to be 0.2%. There, integer values of α were considered, and here we have assigned a somewhat larger numerical uncertainty (0.4%)

to the present exp/6 collision integrals, principally arising from our interpolation to non-integer values of α.

The error associated with the potential energy surface is the largest source of error in D, arising both from fitting errors in the analytic surface and errors in the quantum chemistry method on which the fitted surface is based. While the fitting error may be larger along some cuts through the intermolecular potential, Fig 1(a) shows that the spherically-averaged intermolecular potentials for the directly calculated QCISD(T)/CBS potential and for the fitted surface are in good agreement with one another, although there are small differences high up the repulsive wall. One may therefore obtain exp/6 parameters for the directly calculated QCISD(T)/CBS energies (α = 11.45, σ = 3.35 Å, and ε = 27.0 cm^{-1}) that differ slightly from those for the fitted surface (α = 11.6, σ = 3.36 Å, and ε = 26.1 cm^{-1}). Diffusion coefficients calculated for these two exp/6 potentials differed by less than 0.4% up to 1500 K and by 0.8% at 3000 K, with the direct result systematically higher than that of the fitted potential.

The error associated with the choice of quantum chemistry method is considered next. Energies obtained using the counterpoise corrected QCISD(T)/CBS method that was used to fit the present analytic surface were compared with the results of a high-level (HL) method defined as follows: CCSD(T) energies were extrapolated to the CBS limit using a two-point formula and the aug-cc-pV5Z and aug-cc-pV6Z basis sets. The CBS extrapolation was carried out with and without counterpoise corrections, and the two CBS energies were averaged. A high-level correction was added that included core-valence, relativistic, geometry relaxation, and higher-order excitation (including up to full quadruples and perturbative pentuples excitations, TQ(P)) corrections. The core-valence correction was obtained from CBS extrapolation of calculations for cc-pCVTZ and cc-pCVQZ basis sets, the relativistic correction employed a cc-pVTZ basis set, the geometry relaxation employed the cc-pVQZ basis set, and T(Q) and Q(P) corrections employed the cc-pVTZ and cc-pVDZ basis sets, respectively. The QCISD(T)/CBS and HL energies were calculated along two cuts (T-shaped and linear) through the interaction potential, with very similar relative differences between the two methods along each cuts. The interaction energies for the two methods differed by less than 1.5 cm^{-1} near the van der Waals minimum (corresponding to 4% errors in ε), by less than 3 cm^{-1} near the inner

turning point (corresponding to 0.5% errors in σ), and by 5–15 cm^{-1} around 1000 cm^{-1} up the repulsive wall (corresponding to 0.5% errors in α). Collision integrals were evaluated for exp/6 fits to the QCISD(T)/CBS and HL curves along both of the cuts. The computed (1,1) collision integrals for the two quantum chemistry methods differed from one another by less than 0.3%.

Error bars for the calculated HL intermolecular potential method were estimated and represent any small but remaining incomplete basis set and correlation effects. The error bars were assumed to be comprised of independent contributions from the full high-level correction and from one-half of the difference in the CBS extrapolations with and without the counterpoise correction. The resulting error bars are approximately half as large as the QCISD(T)/CBS and HL differences identified above. The effect of these small errors in the HL potential on the computed collision integrals was therefore estimated to be smaller than those associated with numerical errors. Considering errors arising from both the fitted potential and from the choice of quantum chemistry method, we estimated 2-sigma error bars associated with the potential energy surface to be 0.6%.

The preceding error analysis was used to both improve the present calculated value of D and to provide first-principles error bars. Two important systematic errors were identified above: the quantum correction, which increased D by up to 0.8% at low T, and the fitting error in the analytic potential at high repulsive energies, which increased D by up to 0.8% at high T. The two corrections were considered additive, and an improved value of D was obtained by scaling the results of eq 4 accordingly. The improved values of D were increased relative to the results of eq 4 by 1% at 300 K, by 0.4% at 1000 K, and by 0.8% at 3000 K. A three-parameter analytic expression fit to the improved theoretical results is given by eq 8 and reproduces the calculated values to within 0.4%. This expression may be assigned 2-sigma first-principles error bars of 0.7% based on those arising from statistical uncertainty (0.4%) and from errors in the fitted potential (0.6%), as detailed above. For comparison with other workers, we note that the best two parameter fit to the improved calculated values of D at 1 atm is 1.236 (T/300 K)$^{1.752}$ cm^2/s, although this expression reproduces the calculated values with errors as large as 2%, which is larger than the present estimated 2-sigma error bars.

Figure 1

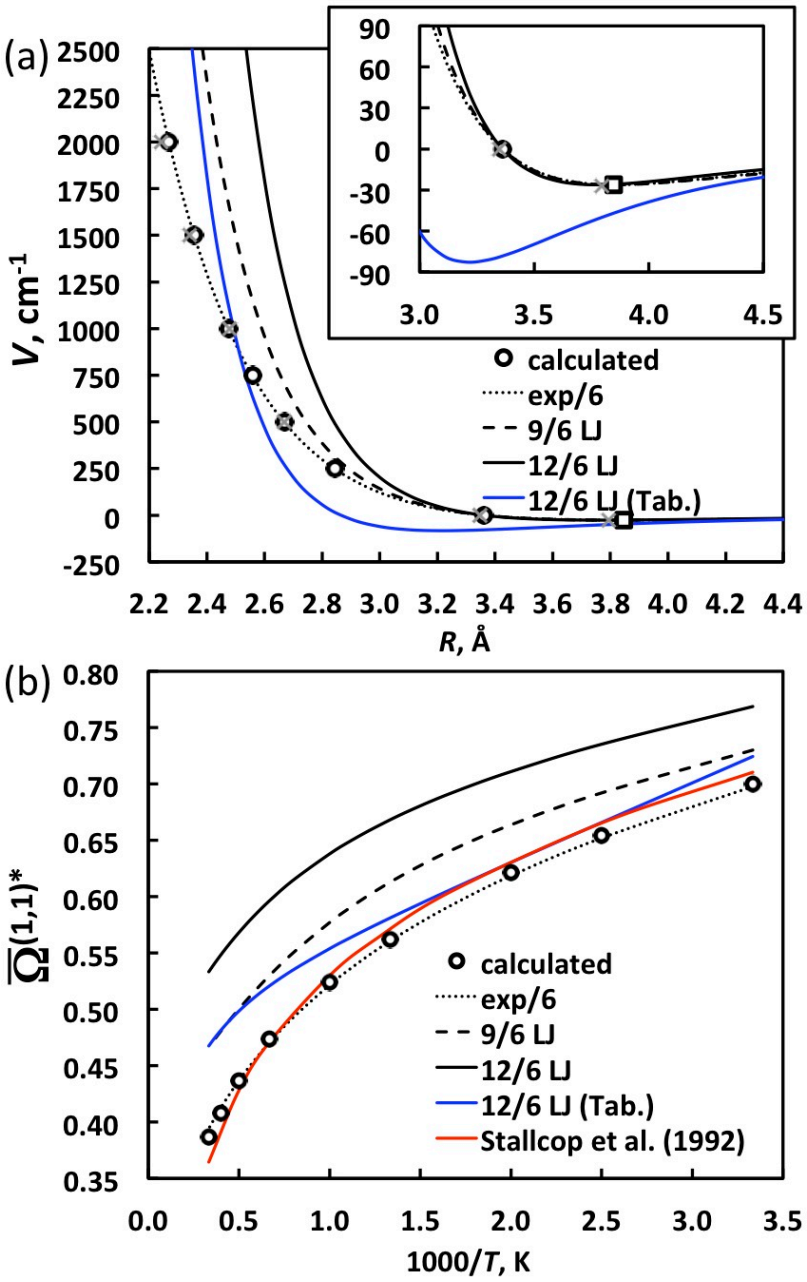

Fig. 1. (a) Isotropic intermolecular potential for H + N_2. The circles are the result of spherical averaging over the full-dimensional analytic potential, and the square indicates the spherically-averaged well depth and distance. Selected direct results for the QCISD(T)/CBS surface are shown as gray x's. 9/6 and 12/6 Lennard–Jones potentials based on the calculated values of σ and ε are also shown, along with an optimized exp/6 potential (black lines). The blue line is the 12/6 Lennard–Jones potential obtained using tabulated parameters. The inset highlights the van der Waals well. (b) Reduced (1,1) collision integrals for the isotropic potential curves shown above (black and blue lines) and for the full-dimensional classical results of eq 4 (circles with 2-sigma statistical error bars). Also shown are the semiclassical scattering results of Stallcop et al.[13] (red line). All of the curves shown in (b) were reduced to the collision radius $\overline{\sigma}$ = 3.36 Å to enable a direct comparison of the methods.

Figure 2

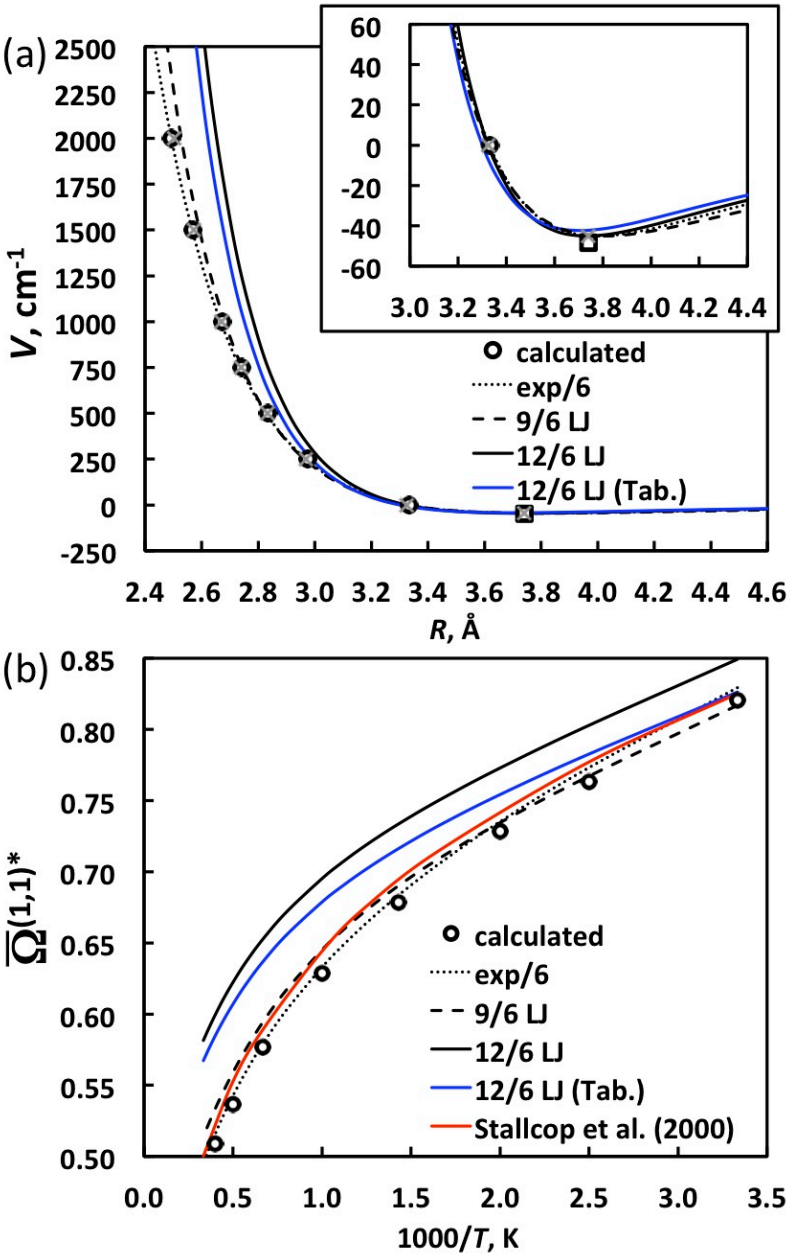

Fig. 2. (a) Isotropic intermolecular potential and (b) reduced (1,1) collision integral for H_2 + N_2. The meanings of the symbols and lines are the same as in Fig. 1. The semiclassical scattering results of Stallcop et al.[14] are shown as a red line. All of the curves shown in (b) were reduced to the collision radius $\bar{\sigma}$ = 3.32 Å to enable a direct comparison of the methods.

Figure 3

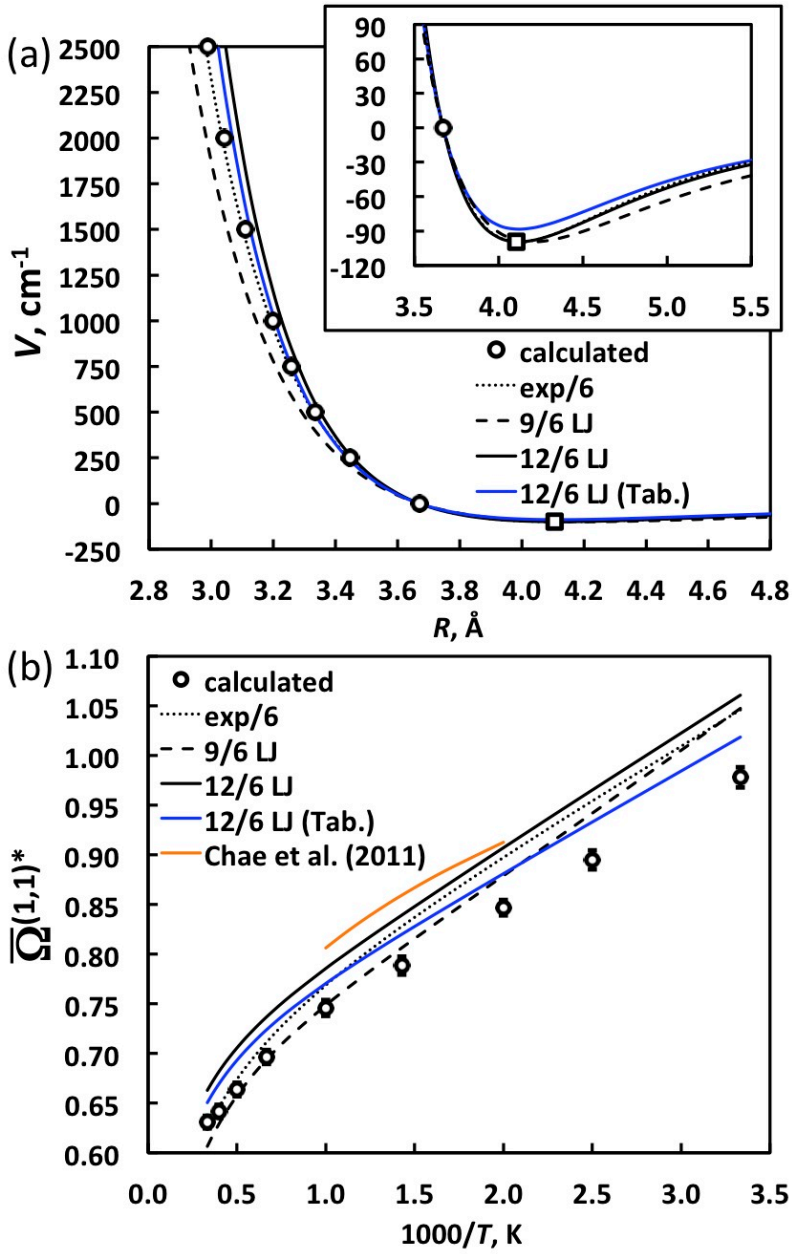

Fig. 3. (a) Isotropic intermolecular potential and (b) reduced (1,1) collision integral for CH_4 + N_2. The meanings of the symbols and lines are the same as in the previous figures. Also shown are the previous molecular dynamics results of Chae et al.[30] (orange line). All of the results in (b) were reduced to the collision radius $\bar{\sigma}$ = 3.67 Å to enable straightforward comparisons of the methods.

Figure 4

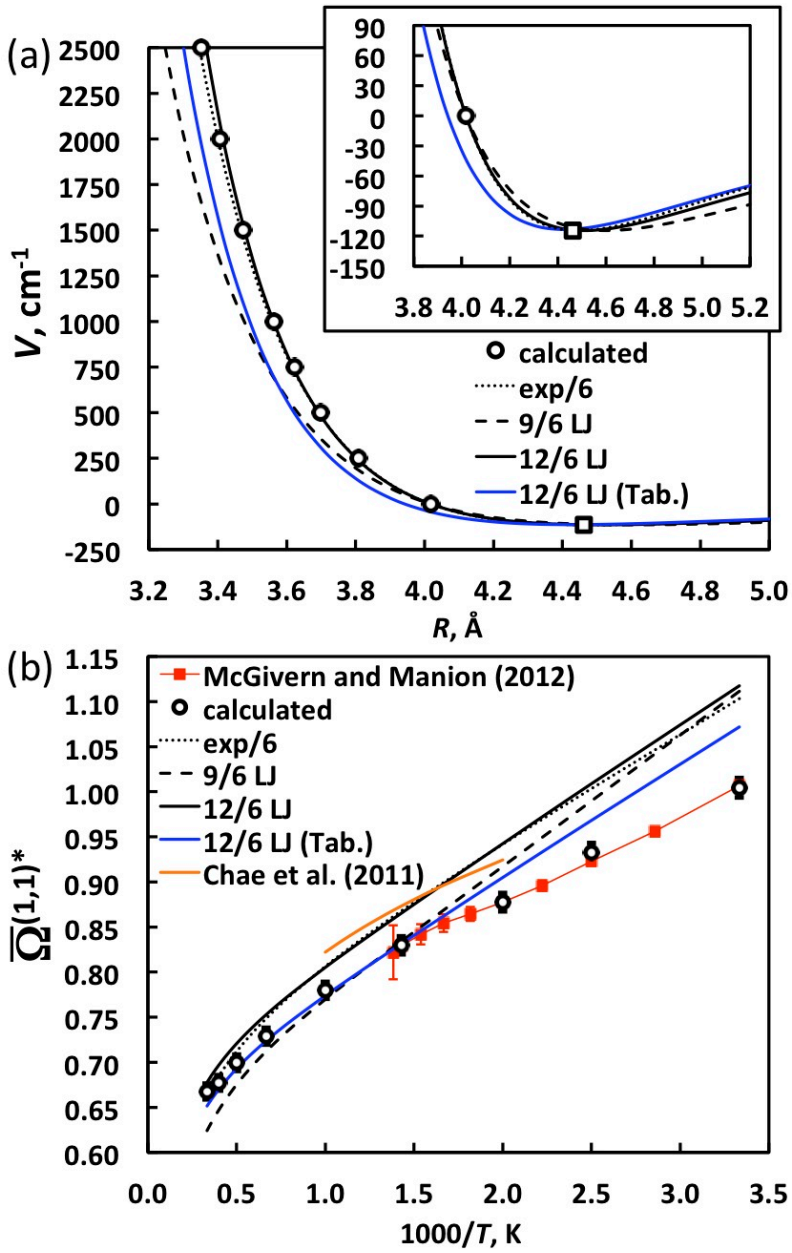

Fig. 4. (a) Isotropic intermolecular potential and (b) reduced (1,1) collision integrals for C_2H_6 + N_2. The meanings of the symbols and lines are the same as in the previous figures. Also shown are the experimental collision integrals of McGivern and Manion (red squares).[21] All of the results in (b) were reduced to the collision radius $\bar{\sigma}$ = 4.02 Å to enable straightforward comparisons of the methods.

Figure 5

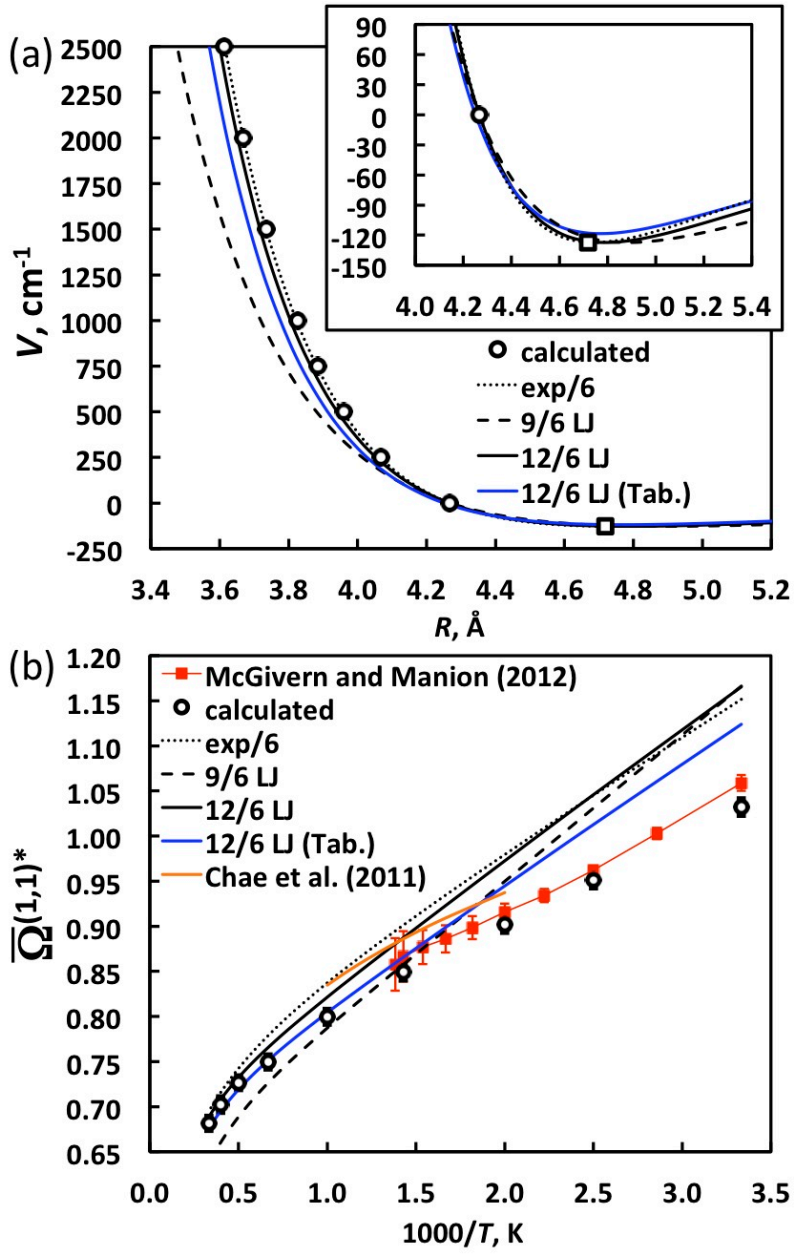

Fig. 5. (a) Isotropic intermolecular potential and (b) reduced (1,1) collision integrals for C_3H_8 + N_2. The meanings of the symbols and lines are the same as in the previous figures. All of the results in (b) were reduced to the collision radius $\bar{\sigma}$ = 4.27 Å to enable straightforward comparisons of the methods.

Figure 6

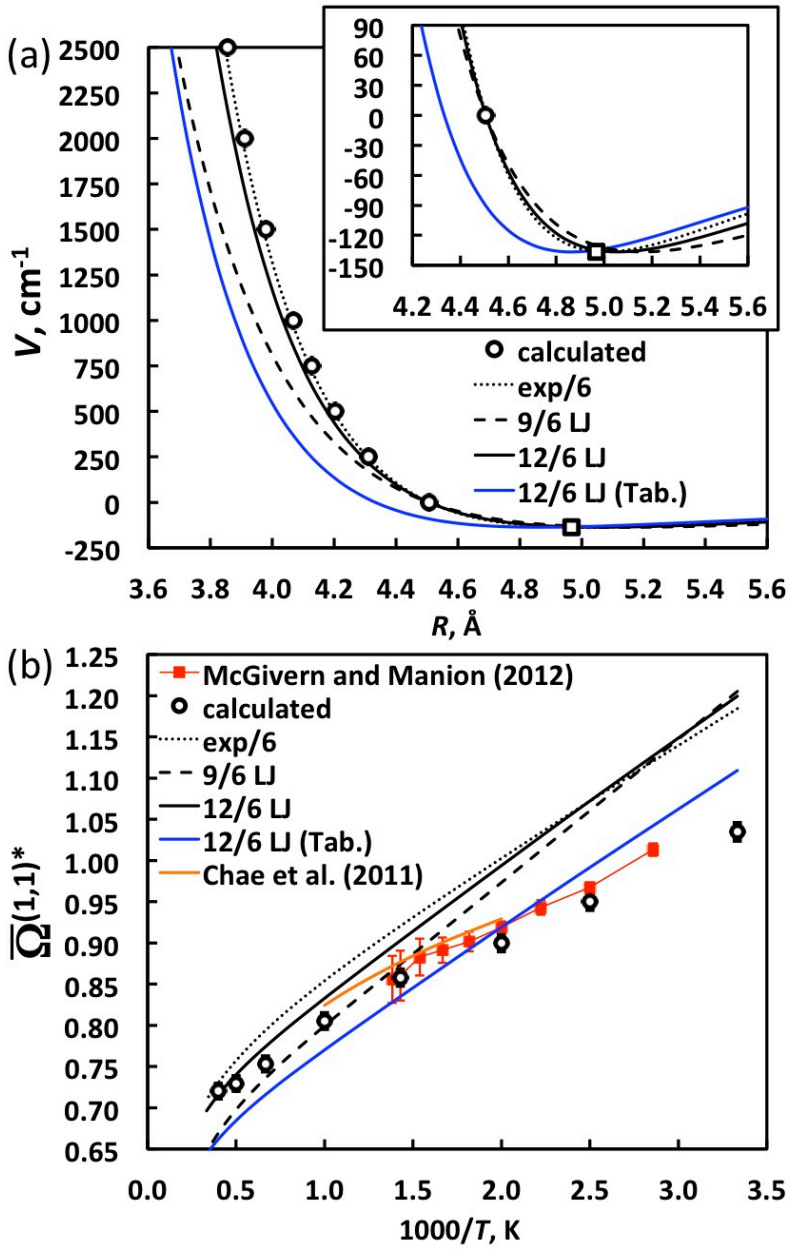

Fig. 6. (a) Isotropic intermolecular potential and (b) reduced (1,1) collision integrals for C_4H_{10} + N_2. The meanings of the symbols and lines are the same as in the previous figures. All of the results in (b) were reduced to the collision radius $\bar{\sigma}$ = 4.51 Å to enable straightforward comparisons of the methods.

Figure Captions

Fig. 1. (a) Isotropic intermolecular potential for H + N_2. The circles are the result of spherical averaging over the full-dimensional analytic potential, and the square indicates the spherically-averaged well depth and distance. Selected direct results for the QCISD(T)/CBS surface are shown as gray x's. 9/6 and 12/6 Lennard–Jones potentials based on the calculated values of σ and ε are also shown, along with an optimized exp/6 potential (black lines). The blue line is the 12/6 Lennard–Jones potential obtained using tabulated parameters. The inset highlights the van der Waals well. (b) Reduced (1,1) collision integrals for the isotropic potential curves shown above (black and blue lines) and for the full-dimensional classical results of eq 4 (circles with 2-sigma statistical error bars). Also shown are the semiclassical scattering results of Stallcop et al.[13] (red line). All of the curves shown in (b) were reduced to the collision radius $\bar{\sigma}$ = 3.36 Å to enable a direct comparison of the methods.

Fig. 2. (a) Isotropic intermolecular potential and (b) reduced (1,1) collision integral for H_2 + N_2. The meanings of the symbols and lines are the same as in Fig. 1. The semiclassical scattering results of Stallcop et al.[14] are shown as a red line. All of the curves shown in (b) were reduced to the collision radius $\bar{\sigma}$ = 3.32 Å to enable a direct comparison of the methods.

Fig. 3. (a) Isotropic intermolecular potential and (b) reduced (1,1) collision integral for CH_4 + N_2. The meanings of the symbols and lines are the same as in the previous figures. Also shown are the previous molecular dynamics results of Chae et al.[30] (orange line). All of the results in (b) were reduced to the collision radius $\bar{\sigma}$ = 3.67 Å to enable straightforward comparisons of the methods.

Fig. 4. (a) Isotropic intermolecular potential and (b) reduced (1,1) collision integrals for C_2H_6 + N_2. The meanings of the symbols and lines are the same as in the previous figures. Also shown are the experimental collision integrals of McGivern and Manion (red squares).[21] All of the results in (b) were reduced to the collision radius $\bar{\sigma}$ = 4.02 Å to enable straightforward comparisons of the methods.

Fig. 5. (a) Isotropic intermolecular potential and (b) reduced (1,1) collision integrals for C_3H_8 + N_2. The meanings of the symbols and lines are the same as in the previous figures. All of the results in (b) were reduced to the collision radius $\bar{\sigma}$ = 4.27 Å to enable straightforward comparisons of the methods.

Fig. 6. (a) Isotropic intermolecular potential and (b) reduced (1,1) collision integrals for C_4H_{10} + N_2. The meanings of the symbols and lines are the same as in the previous figures. All of the results in (b) were reduced to the collision radius $\bar{\sigma}$ = 4.51 Å to enable straightforward comparisons of the methods.

References

[1] J. O. Hirschfelder, C. F. Curtiss, R. B. Bird, R. B. Molecular Theory of Gases and Liquids (Wiley, New York, 1954).

[2] E. A. Mason, "Transport in Neutral Gases," in *Kinetic Processes in Gases and Plasmas*, edited by A. R. Hochstim (Academic Press, London, 1969), pp. 57–97.

[3] G. C. Maitland, M. Rigby, E. B. Smith, and W. A. Wakeham, Intermolecular Forces: Their Origin and Determination (Clarendon, Oxford, 1987).

[4] S. Chapman and T. G. Cowling, The Mathematical Theory of Non-Uniform Gases (Cambridge University Press, New York, 1952).

[5] M. Klein and F. J. Smith, *J. Res. Nat. Bureau Standards. A. Phys. Chem.* **72A**, 359 (1968).

[6] N. J. Brown, L. A. J. Bastian, and P. N. Price, *Prog. Energy Combust. Sci.* **37**, 565 (2011).

[7] R. J. Kee, F. M. Rupley, J. A. Miller, M. E. Coltrin, J. F. Grcar, E. Meeks, H. K. Moffat, A. E. Lutz, G. Dixon-Lewis, M. D. Smooke, J. Warnatz, G. H. Evans, R. S. Larson, R. E. Mitchell, L. R. Petzold, W. C. Reynolds, M. Caracotsios, W. E. Stewart, P. Glarborg, C. Wang, C. L. McLellan, O. Adigun, W. G. Houf, C. P. Chou, S. F. Miller, P. Ho, P. D. Young, D. J. Young, D. W. Hodgson, M.V. Petrova, K. V. Puduppakkam, CHEMKIN, Reaction Design, San Diego, CA, 2010.

[8] A. W. Jasper and J. A. Miller, *Combust. Flame*, **161**, 101 (2014).

[9] N. Taxman, *Phys. Rev.* **110**, 1235 (1958).

[10] C. S. Wang Chang and G. E. Uhlenbeck, "Transport Phenomena in Polyatomic Gases," University of Michigan Engineering Research Rept. No. CM-681, July 1951.

[11] S. Imam-Rahajoe, C. F. Curtiss, and R. B. Bernstein, *J. Chem. Phys.* **42**, 530 (1965).

[12] J. M. Hutson and F. R. McCourt, *J. Chem. Phys.* **80,** 1135 (1983).

[13] J. R. Stallcop, H. Partridge, S. P. Walch, and E. Levin, *J. Chem. Phys.* **97**, 3431 (1992).

[14] J. R. Stallcop, H. Partridge, and E. Levin, *Phys. Rev. A* **62**, 062709 (2000).

[15] P. Middha, B. Yang, and H. Wang, *Proc. Combust. Inst.* **29**, 1361 (2002).

[16] P. J. Dagdigian and M. H. Alexander, *J. Chem. Phys.* **138**, 164305 (2013).

[17] P. J. Dagdigian and M. H. Alexander, *J. Chem. Phys.* **139**, 194309 (2013).

[18] L. Monchick, K. S. Yun, and E. A. Mason, *J. Chem. Phys.* **38**, 1282 (1963).

[19] E. A. Mason, *J. Chem. Phys.* **22**, 169 (1954).

[20] F. J. Smith and R. J. Munn, *J. Chem. Phys.* **41**, 3560 (1964).

[21] W. S. McGivern and J. A. Manion, *Combust. Flame* **159**, 3021 (2012).

[22] A. W. Jasper and J. A. Miller, *J. Phys. Chem. A* **113**, 5612 (2009).

[23] B. Efron, *Ann. Stat.* **7**, 1 (1979).

[24] S. Nangia, A. W. Jasper, T. F. Miller, and D. G. Truhlar, *J. Chem. Phys.* **120**, 3586 (2004).

[25] A. W. Jasper, C. M. Oana, and J. A. Miller, *Proc. Combust. Inst.* **35** (2015), in press (doi:10.1016/j.proci.2014.05.105).

[26] A. W. Jasper and J. A. Miller, *J. Phys. Chem. A* **115**, 6438 (2011).

[27] B. J. Braams and J. M. Bowman, *Int. Rev. Phys. Chem.* **28**, 577 (2009).

[28] Y. Paukku, K. R. Yang, Z. Varga, and D. G. Truhlar, *J. Chem. Phys.* **139**, 044309 (2013), **140**, 019903(E) (2014).

[29] R. Conte, P. L. Houston, and J. M. Bowman, *J. Chem. Phys.* **140**, 151101 (2014).

[30] K. Chae, P. Elvati, and A. Violi, *J. Phys. Chem. B* **115**, 500 (2011).

[31] M. S. Green, J. *Chem. Phys.* **22**, 398 (1954). R. Kubo, *J. Phys. Soc. Jpn.* **12**, 570 (1957).

[32] L. S. Tee, S. Gotoh, and W. E. Stewart, *I&EC Fundamentals* **5**, 356 (1966).

[33] Q. Ma, P. J. Dagdigian, and M. H. Alexander, *J. Chem. Phys.* **138**, 104317 (2013).